



# Common Carotid Artery Lumen Automatic Segmentation from Cine Fast Spin Echo Magnetic Resonance Imaging

Lívia Rodrigues<sup>1</sup>(✉), Roberto Souza<sup>2</sup>, Letícia Rittner<sup>1</sup>, Richard Frayne<sup>2</sup>,  
and Roberto Lotufo<sup>1</sup>

<sup>1</sup> Faculty of Electrical and Computer Engineering, University of Campinas,  
Campinas, Brazil

lmarodr@dca.fee.unicamp.br

<sup>2</sup> Departments of Radiology and Clinical Neuroscience, University of Calgary,  
Calgary, Canada

**Abstract.** Atherosclerosis is one of the main causes of stroke and is responsible for millions of deaths every year. Magnetic resonance (MR) is a common way of assessing carotid artery atherosclerosis. Cine fast spin echo (FSE) imaging is a new MR method that can now obtain dynamic image data of the carotid artery across the cardiac cycle. This work introduces a post-processing technique that segments the common carotid artery (CCA) wall-blood boundary across the cardiac cycle without human interaction. To the best of our knowledge, the proposed method is the first automatic technique proposed for segmenting cardiac cycle-resolved cine FSE images. The technique overcomes some inherent limitations of dynamic FSE images compared to static images (*e.g.*, lower spatial resolution). It combines *a priori* knowledge about the size and shape of the CCA, with the max-tree data structure, random forest classifier and tie-zone watershed transform from identified internal and external markers to segment the vessel lumen. Segmentation performance was assessed using 3-fold cross validation with 15 cine FSE data sets in the test set per fold, each sequence consisting of 16 temporal bins over the cardiac cycle. The automatic segmentation was compared against manually segmented images. Our technique achieved an average Dice coefficient, sensitivity and false positive rate of  $0.926 \pm 0.005$  (mean  $\pm$  standard deviation),  $0.909 \pm 0.011$  and  $0.056 \pm 0.003$ , respectively, compared to the majority voting consensus of manual segmentation from three experts.

**Keywords:** Max-tree · Tie-zone watershed · Carotid artery ·  
Cine FSE imaging

## 1 Introduction

It is estimated that 4.4 million people die every year because of stroke [14], making it one of the most common causes of death in the developed world.

Atherosclerosis is a major cause of stroke and is attributed to about 25% of all ischemic events [10]. Currently there are several different types of examinations used to identify carotid atherosclerotic plaques and analyze the artery including ultrasound and x-ray. However, these techniques are generally limited by poor blood-wall image contrast [4,9]. Magnetic resonance (MR) imaging provides improved tissue contrast between vessel wall and lumen [14].

For this project we used cine fast spin echo (FSE) imaging, which differs from usual FSE imaging in that this method collects dynamic information about distension and contraction of carotid artery over the cardiac cycle. Standard MR imaging techniques usually acquire images with good tissue contrast, however, they can be affected by motion artifacts, particularly when needing long acquisition times [9]. Cine FSE imaging, on the other hand, is capable of acquiring a set of  $N$  of images ( $N$  usually between 10 and 20) over the cardiac cycle in approximately the same acquisition time used by a standard FSE technique to acquire one static image [4,9].

Current carotid artery segmentation methods [2,11,13] use static carotid MR images *i.e.*, there is no temporal information. In addition in most published methods, some degree of human interaction is required. In the present work, we focus on a fully automatic segmentation of the common carotid artery (CCA) lumen, *i.e.*, the interior of the CCA, from cine FSE images. Our segmentation method uses the max-tree [12] area signature analysis combined with tie-zone watershed [3] and random forest classifier [5] to achieve accurate segmentations.

This paper is organized as follows: Sect. 2 describes cine FSE image and proposed solution. Section 3 details the data set and experiments. Sections 4 and 5 present results, discussions and conclusions of this paper.

## 2 Materials and Methods

### 2.1 Cine FSE Images

Conventional static MR FSE imaging techniques generate images with acceptable vessel wall-blood image contrast and allows for the depiction of vessel wall morphology and characterization of plaque components. FSE images, with proton density-, T1- and/or T2-weightings are commonly used [10, 14]. These images provide only a snap-shot (*i.e.*, they are time averaged) of the vessel wall morphology and composition over the cardiac cycle. They can also suffer from cardiac motion-induced artifacts due to their long data acquisition times [9]. Cine FSE imaging is a new technique that is capable of acquiring images across the cardiac cycle in total acquisition times similar to those required for a standard static FSE technique, albeit often with slightly reduced spatial resolution [4,9]. Because cine FSE images are resolved over the cardiac cycle they potentially can increase its accuracy and reduce image artifacts due to blood flow and wall motion [4].

Cine FSE acquires data over the entire acquisition window asynchronously with respect to the contraction of the heart. The acquired raw MR data is however tagged with its acquisition time within the cardiac cycle (typically using

information from a pulse oximeter). The raw data is then rebinned into  $N$  temporal bins that evenly cover the average cardiac cycle.  $N$  is user selectable and in this study  $N = 16$ . Because the raw MR data was collected asynchronously, each rebinned data set will, in general, be incomplete. Therefore sophisticated, non-linear reconstruction methods, based on compressed sensing [8], are required to generate images. Compared to static FSE images, cine FSE images are able to generate a similar range of image contrasts (weightings), with potentially lower resolution and signal-to-noise, but fewer flow and motion artifacts. The cine FSE data acquisition process is fully explained in Boesen *et al.* [4] and is a refinement of the method developed in [9].

## 2.2 Proposed Method

Our solution uses appropriate size and shape information obtained from the max-tree algorithm to find the CCA centroid, internal and external (to the carotid artery lumen) markers, which then are used by the tie-zone watershed transform. The proposed method has five main steps detailed in Fig. 1.

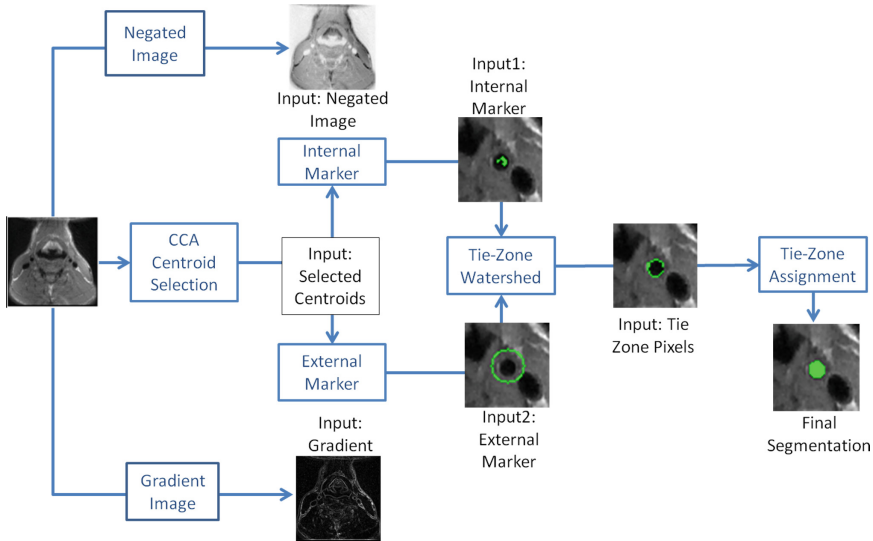
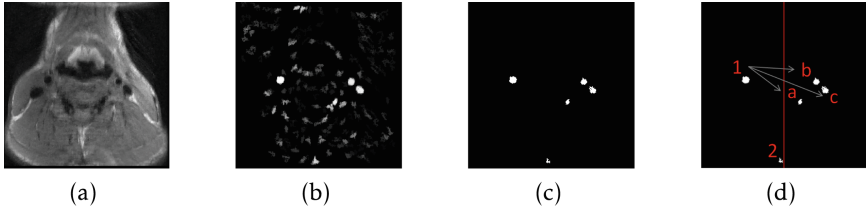


Fig. 1. Flowchart of proposed method.

1. **CCA Centroid Selection:** The first step of the method performs the automatic selection of the left and right CCA centroids. For this task, we use the max-tree for image filtering combined with feature extraction and random forest classification for final selection (Fig. 2).



**Fig. 2.** Illustration of the centroid selection procedure: (a) Original image, (b) probability image (c) binary image, and (d) Final 6 pairs of centroids: 1-a, 1-b, 1-c, 2-a, 2-b and 2-c.

- (a) *Max-Tree Filtering*: Initially, we use a max-tree filter to return only the nodes with area between  $14.5 \text{ mm}^2$  and  $46.6 \text{ mm}^2$  [7]. This filter is applied over all 16 temporal bins reconstructed by the cine FSE sequence.
  - (b) *Probability Image and Binary Image*: A probability image is created by summing over all 16 filtered images from the previous step. Next, we applied a threshold of 0.8 to the probability image, therefore maintaining only pixels that appeared in more than 80% of the 16 filtered images, resulting in a binary image containing the candidate nodes (Fig. 2).
  - (c) *Feature Extraction*: Using the binary image, we perform feature extraction from its connected components (CCs), which are the “white islands” in the binary image. The attributes analyzed consist of the corresponding gray level in the original unfiltered image, area, eccentricity, centroid of CCs and distance between pairs of CCs. In order to create a feature matrix, we divided the final image into a left side and right side and analyzed the identified structures by pairs (Fig. 2(d)). At the end of this step, we have a feature matrix of dimension  $n \times 11$ , with  $n$  being the number of candidate pairs returned in the image. The feature matrix is the input to the classifier.
  - (d) *Classifier*: We use a random forest (RF) classifier with 45 estimators, operating with entropy criteria to automatically detect the centroids. The classifier outputs probabilities for each candidate pair of centroids. The pair with highest probability is considered the carotid centroids’.
2. **Internal Marker Selection**: The internal marker (IM) selection uses *a priori* knowledge of carotid artery area and one assumption about cine FSE images. These assumptions are: (1) the carotid artery diameter varies from 4.4 mm to 7.7 mm [7] and (2) the histogram of two consecutive temporal images are similar (Fig. 3(f).) In selecting the IM we are interested in the carotid lumen which is dark in the cine FSE image. Therefore, we built the max-tree of the negative image (*i.e.*, the min-tree), then, we analyzed the min-tree area signature starting from the selected centroid to the min-tree root. Finally, we created a filter using *a priori* knowledge about the CCA area ( $14.5 \text{ mm}^2$  to  $46.6 \text{ mm}^2$  [7]), reducing the number of max-tree nodes that need to be analyzed (Fig. 3(a-e)). From the final candidate nodes, the IM was selected based on our histogram similarity assumption. We selected

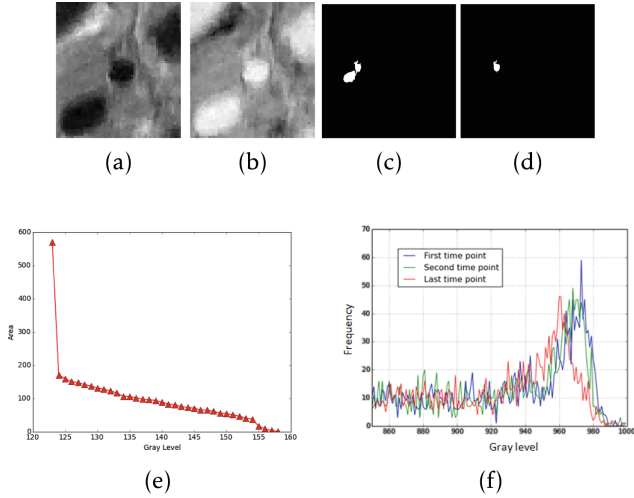


**Fig. 3.** (a) Original image (b) Negated image (c) Image representing the node before the decrease in max-tree signature, see (e). (d) Image representing the node after the decrease in max-tree signature. (e) Max-tree signature from the negated image for structures smaller than  $46.6 \text{ mm}^2$ . After the decrease, only the carotid artery lumen and wall are represented. (f) Intensity histograms for region around carotid artery from the same slice at different time points (Kolmogorov-Smirnov test found no significant differences between the three histograms,  $p = 0.918$ ).

as an IM marker the candidate with gray-level value closest to the gray level of the previous time point. For the first temporal bin, we selected the node with gray level closest to the peak value of the histogram, assuming that the vessels are the brightest structures in the negated image.

3. **External Marker Selection:** For external markers (EM), we are interested in the vessel wall, which is the brighter structure immediately surrounding the lumen (Fig. 4). To select the EM, we built the max-tree of the gradient image to find nodes around the carotid artery lumen. We use the gradient image because it accentuates the artery wall-lumen boundary. We choose the node whose centroid has the smallest Euclidean distance to the CCA centroid. Usually, the carotid artery wall is not entirely represented by a single max-tree node (*cf.* Figure 4(b)). The EM will work better if it encloses the carotid lumen; therefore, the final EM was composed of a circle of diameter equal to  $1.5 \times$  the largest distance between the pixels of the selected max-tree node and the CCA centroid. The selected diameter was not allowed to exceed 7.7 mm, the assumed maximum diameter for the CCA [7], in order to prevent leakage into the tie-zone watershed transform.
4. **Tie-Zone Watershed:** The tie-zone watershed transform receives the automatically selected IM and EM as input and it is applied to the gradient image. The tie-zone watershed returns regions of doubt that have the same cost value for both the lumen and vessel wall labels. These pixels, known as “tie-zone”

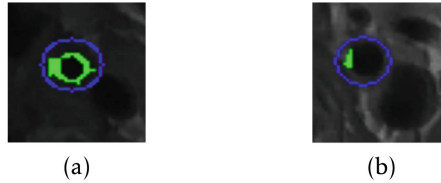


**Fig. 4.** Two illustrative cases for finding the external marker (EM): (a) Case where a Node represents the entire vessel wall (green) and the final external marker (blue). (b) Case where there is no node representing the entire vessel wall (green) and the final external marker (blue). (Color figure online)

pixels, need to be correctly assigned in order to improve the accuracy of the method.

5. **Tie-Zone Assignment:** The tie-zone pixels are assigned using a RF classifier with 30 estimators, operating with entropy criteria. The classification was performed on a pixel-by-pixel basis using features extracted from each tie-zone pixel (local binary pattern (LBP) [1], histogram of gradients (HOG) [6], tie-zone labels histogram, gray level of the pixel and mean gray level of 8-neighbors around the pixel). The two histograms (tie-zone histogram and HOG) were computed on a  $3 \times 3$  pixel window centered about the tie-zone pixel. All features were computed on the original cine FSE image.

### 3 Experimental Setup

Our data set is composed of 9 healthy subjects, each subject having 5 different MR image acquisitions. Therefore, we have a total of 45 data sets, each with  $N = 16$  temporal bins and a resolution of  $0.6 \text{ mm} \times 0.6 \text{ mm} \times 2.0 \text{ mm}$ . We performed two experiments to validate our proposed method: the first related to the automatic centroid selection and the second related to the CCA lumen segmentation.

*Experiment 01 - CCA Centroid Selection:* For the CCA centroid selection we used 20 data sets for training and validation of the RF classifier and 25 data sets for testing the classifier. On the training and validation set, we applied data augmentation by applying scale, rotation, and translation transformations to the images, in order to increase the classifier robustness. After data augmentation, our training and validation data set was composed of 105 image data sets. The centroid selection was assessed through the classifier accuracy. The test set and training/validation set were composed by different subjects images, in order to avoid bias towards high performance results.

*Experiment 02 - CCA Lumen Segmentation:* In the CCA lumen segmentation experiment we used a k-fold, with  $k = 3$ , cross-validation to assess our method. Each of the folds is composed of 15 images from 3 different subjects. For each image data set we obtained manual segmentation from three different experts

(Experts 1, 2 and 3) for validation purposes of our method. A majority voting consensus was used to assess our results. We used the Dice coefficient, sensitivity and false positive rate (FPR) metrics.

## 4 Results and Discussion

In the centroid selection experiment, we achieved an accuracy of 100%. In some cases more than one pair of candidate nodes had a probability higher than 50%, but by selecting only the pair with highest probability, this issue was overcome.

For the segmentation experiment, the average and standard-deviation of the cross-validation results are summarized in Table 1. Overall, good visual agreement was observed between our method and the voting consensus of the experts’ segmentation (Fig. 5). Our Dice coefficient was 0.926 when assessed against the voting consensus results. Similarly good performance was observed for sensitivity and FPR. [13] reported a dice coefficient of 0.93 when using static FSE images. Despite a marginally lower Dice coefficient, our findings are encouraging because they account for the fact that our data set is more challenging as cine FSE images have lower resolution, and our method is fully automated. Perhaps not surprising given the newness of the cine FSE [4]. We could not find any public segmentation method to directly compare with our method.

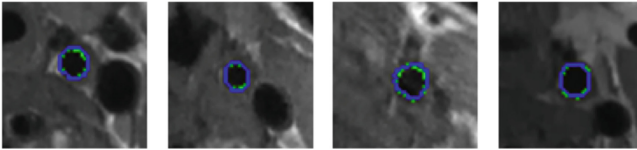


**Fig. 5.** Representative images. Our segmentation (shown in green) agrees with the voting consensus (in blue). (Color figure online)

**Table 1.** Dice coefficient, sensitivity and false positive rate (FPR) metrics. Averages (mean  $\pm$  standard deviation shown) across all three folds are reported comparing automatic segmentation (AS) against the manual segmentation majority voting consensus (VC) and the three experts (Exp  $m$ ,  $m = 1, 2$ , or 3).

	Dice	Sensitivity	FPR
AS x VC	0.926 $\pm$ 0.005	0.909 $\pm$ 0.011	0.056 $\pm$ 0.003
AS x Exp 1	0.906 $\pm$ 0.011	0.923 $\pm$ 0.005	0.057 $\pm$ 0.003
AS x Exp 2	0.905 $\pm$ 0.009	0.896 $\pm$ 0.010	0.084 $\pm$ 0.007
AS x Exp 3	0.914 $\pm$ 0.004	0.900 $\pm$ 0.013	0.071 $\pm$ 0.009
Exp 1 x Exp 2	0.918 $\pm$ 0.008	0.921 $\pm$ 0.005	0.075 $\pm$ 0.005
Exp 1 x Exp 3	0.941 $\pm$ 0.006	0.941 $\pm$ 0.004	0.057 $\pm$ 0.009
Exp 2 x Exp 3	0.908 $\pm$ 0.005	0.908 $\pm$ 0.011	0.057 $\pm$ 0.009

## 5 Conclusions

This work proposes a new methodology for automatic CCA lumen segmentation. There are a number of MR image-based, vessel segmentation methods described in the literature, however, none operate on cine FSE image data sets. In addition, currently available published segmentation methods are semi-automatic; they require some degree of human interaction. Here, we present a fully automatic method, including the CCA centroid selection step. This work is an initial step of a larger project that intends to study carotid artery distensibility (first in the CCA, but then extending to the carotid artery bifurcation, as well as the internal and external artery branches). Based on these findings, we hope to be able to accurately classify carotid artery atherosclerosis patients as healthy (low-risk of stroke) or unhealthy (high-risk of stroke). Cine FSE images are necessary not only for minimizing movement artifacts, but also for allowing the visualization of expansion and contraction of carotid during cardiac cycle, and measurement of carotid artery distensibility.

## References

1. Ahonen, T., Hadid, A., Pietikainen, M.: Face description with local binary patterns: application to face recognition. *IEEE Trans. Pattern Anal. Mach. Intell.* **28**, 2037–41 (2006)
2. Arias-Lorza, A., et al.: Carotid artery wall segmentation in multispectral MRI by coupled optimal surface graph cuts. *IEEE Trans. Med. Imag.* **35**(3), 901–911 (2016)
3. Audigier, R., Lotufo, R.A., Couprie, M.: The tie-zone watershed: definition, algorithm and applications. In: *IEEE International Conference on Image Processing*, vol. 2, pp. II-654-7 (2005)
4. Boesen, M.E., Maior Neto, L.A., Pulwicky, A., Yerly, J., Lebel, R.M.: Fast spin echo imaging of carotid artery dynamics. *Magn. Reson. Med.* **74**(4), 1103–1109 (2015)
5. Breiman, L.: Random forests. *Mach. Learn.* **45**(1), 5–32 (2001)
6. Dalal, N., Triggs, B.: Histograms of oriented gradients for human detection. In: *IEEE CVPR* (2005)
7. Limbu, Y., Gurung, G., Malla, R., Rajbhandari, R., Regmi, S.: Assessment of carotid artery dimensions by ultrasound in non-smoker healthy adults of both sexes. *Nepal Med. Coll.* **8**, 200–203 (2006)
8. Lustig, M., Donoho, D., Pauly, J.M.: Sparse MRI: the application of compressed sensing for rapid MR imaging. *Magn. Reson. Med.* **58**(6), 1182–1195 (2007)
9. Mendes, J., Parker, D., Hulet, J., Treiman, G., Kim, S.: Cine turbo spin echo imaging. *Magn. Reson. Med.* **66**(5), 1286–1292 (2011)
10. Saam, T., et al.: The vulnerable, or high-risk, atherosclerotic plaque: noninvasive MR imaging for characterization and assessment. *Radiology* **244**(1), 64–77 (2007)
11. Sakellarios, A., et al.: Novel methodology for 3d reconstruction of carotid arteries and plaque characterization based upon magnetic resonance imaging carotid angiography data. *Magn. Reson. Imaging* **30**, 1068–82 (2012)
12. Salembier, P., Oliveras, A., Garrido, L.: Antiextensive connected operators for image and sequence processing. *IEEE Tran. Imag. Proc.* **7**(4), 555–570 (1998)



13. Ukwatta, E., Yuan, J., Rajchl, M., Qiu, W., Tessier, D., Fenster, A.: 3-D carotid multi-region MRI segmentation by globally optimal evolution of coupled surfaces. *IEEE Trans. Med. Imag.* **32**, 770–785 (2013)
14. Yuan, C., Mitsumori, L., Beach, K., Maravilla, K.: Carotid atherosclerotic plaque: noninvasive MR characterization and identification of vulnerable lesions. *Radiology* **221**(2), 285–299 (2001)